Electric-field-controlled reversible order-disorder switching of a metal tip surface

Electric-field-controlled reversible order-disorder switching of a metal tip surface

Ludvig de Knoop,[1,*] Mikael Juhani Kuisma,[1,2] Joakim Löfgren,[1] Kristof Lodewijks,[1] Mattias Thuvander,[1] Paul Erhart,[1,†] Alexandre Dmitriev,[1,3,4,‡] and Eva Olsson[1,§]

[1]*Department of Physics, Chalmers University of Technology, 412 96 Gothenburg, Sweden*
[2]*Department of Chemistry, University of Jyväskylä, 40014 Jyväskylä, Finland*
[3]*Department of Physics, University of Gothenburg, 412 96 Gothenburg, Sweden*
[4]*Geballe Laboratory for Advanced Materials, Stanford University, Stanford, California 94305-4045, USA*

(Received 26 October 2017; revised manuscript received 11 June 2018; published 22 August 2018)

While it is well established that elevated temperatures can induce surface roughening of metal surfaces, the effect of a high electric field on the atomic structure at ambient temperature has not been investigated in detail. Here we show with atomic resolution using *in situ* transmission electron microscopy how intense electric fields induce reversible switching between perfect crystalline and disordered phases of gold surfaces at room temperature. *Ab initio* molecular dynamics simulations reveal that the mechanism behind the structural change can be attributed to a vanishing energy cost in forming surface defects in high electric fields. Our results demonstrate how surface processes can be directly controlled at the atomic scale by an externally applied electric field, which promotes an effective decoupling of the topmost surface layers from the underlying bulk. This opens up opportunities for development of active nanodevices in, e.g., nanophotonics and field-effect transistor technology as well as fundamental research in materials characterization and of yet unexplored dynamically controlled low-dimensional phases of matter.

DOI: 10.1103/PhysRevMaterials.2.085006

The interactions of metal surfaces with gases, liquids, solids, and electromagnetic fields are of paramount importance in many fields and their applications, including, but not limited to, catalysis [1,2], plasmonic sensing [3], nano-optics [4], protein mechanics [5], biomolecular interactions [6], and nanoelectronics [7,8]. These interactions are strongly influenced by the surface structure. Such surface interactions are greatly affected by changes in the state of the surface, one example being surface roughening, which is related to surface melting [9–11], a phenomenon that has been discussed for more than a century [12,13]. Surface melting and surface roughening describes the loss of crystallinity (a disordering) of the surface layers while the underlying structure is kept crystalline [9,11]. The first experimental evidence for temperature-induced surface melting was reported in 1985 [14] and was followed by a multitude of observations at elevated temperatures [9–11,15].

Apart from elevated temperatures, the presence of an electric field of sufficient strength can change the state of the surface, e.g., in the form of field-assisted ionization and evaporation of atoms, a phenomenon used in characterization techniques such as field-ion microscopy [16] and atom probe tomography [17,18]. A combination of elevated temperature and a high electric field has also been shown to create a disordered surface [19]. Field evaporation has previously been studied using *in situ* transmission electron microscopy (TEM), a technique that allows simultaneous excitation and observation on the atomic scale, from an ionic liquid [20] and from carbon nanotubes for both reshaping purposes and to improve the properties for electron cold-field emission [21,22]. Cold-field emission is another effect induced by high electric fields (around 2 V/nm [23], whereas field evaporation of gold (Au) commences at around 30 V/nm), utilized in, e.g., electron sources [24] and medical applications. Yet, little is known about the structural dynamics at ambient temperature of metallic surfaces at the atomic level at electric fields *between* the thresholds for cold-field emission and field evaporation. In this paper we report on the dynamics of surface Au atoms in this intermediate electric-field interval. We have directly imaged the effect of the intense electric field on the atomic structure at room temperature using *in situ* TEM. We discovered that the outmost atomic layers switched from order to disorder at fields that were just below the field-evaporation field. The findings are supported by extensive *ab initio* calculations. Further on, we reverted the disordered phase back to the original crystalline form by decreasing the applied electric field, properties that are important for possible utilization in, e.g., field-effect transistors and active nanodevice technologies. Subsequently, by increasing the electric field even further, we also performed and imaged field evaporation at atomic resolution.

The electric field was controlled by a biasing TEM sample holder with a piezo-driven nanomanipulator [25] [left-hand part of Fig. 1(a)] and applied to a Au nanocone [26] with a 1.7 nm tip radius at a chosen distance of 100 nm to the negative cathode. The electric-field strengths were derived from finite-element method modeling taking into account atomic geometry and the applied voltage (Discussion 4 in Supplemental Material, Fig. S3 [27]). By increasing the electrical-field strengths, we observed a change in the atomic structure of the nanocone

*ludvig.deknoop@chalmers.se
†erhart@chalmers.se
‡alexd@physics.gu.se
§eva.olsson@chalmers.se

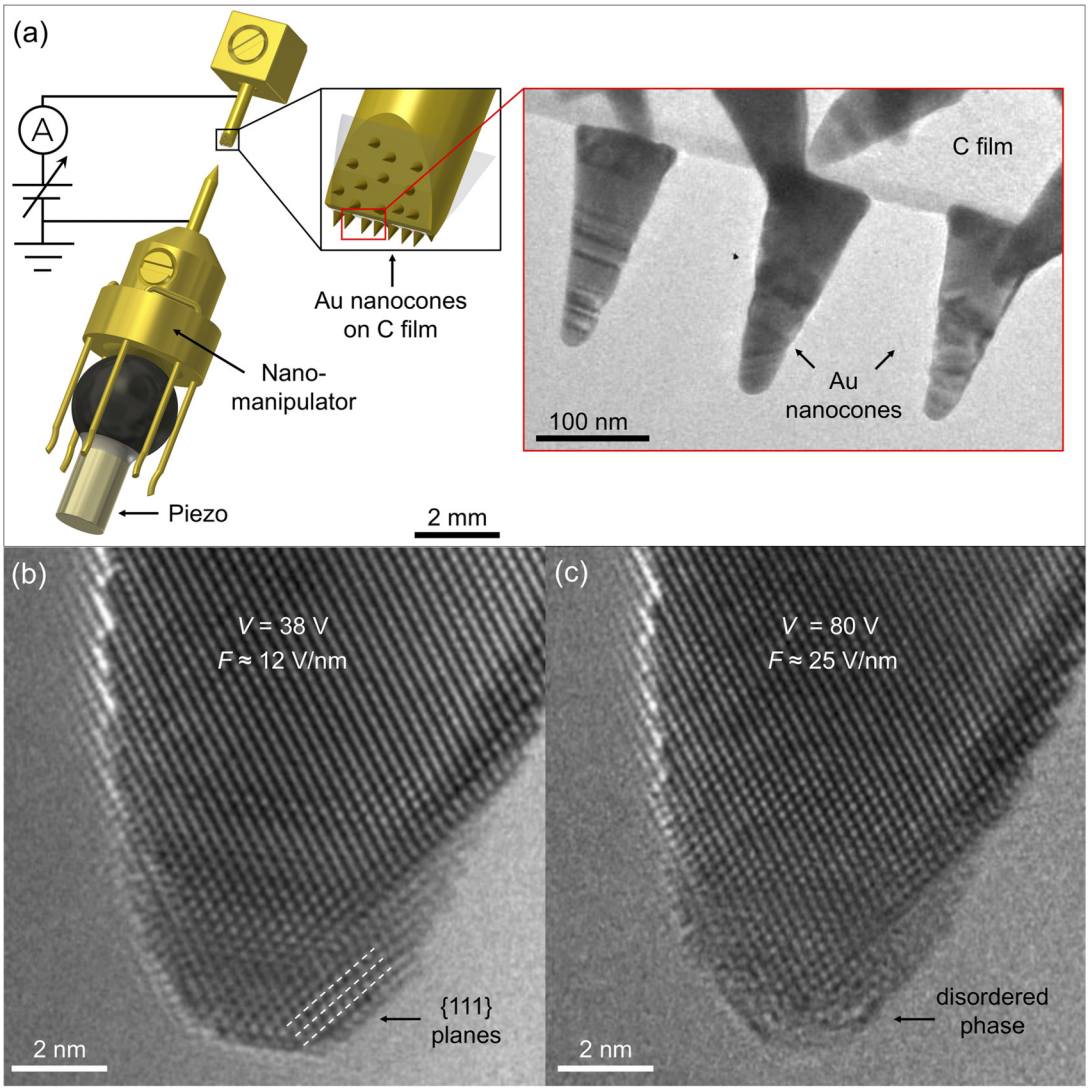

FIG. 1. Experimental setup and results of electric-field-induced order-disorder switching of atomic layers. (a) Schematic of parts of the *in situ* TEM sample holder with the nanomanipulator and the corresponding electrical circuit. The large inset shows a TEM micrograph of the investigated Au nanocones on a carbon (C) film. (b), (c) 10 nm of the apex of one of the nanocones as frames extracted from *In Situ* TEM Movie 2 in Supplemental Material [27]. The disordered phase was switched off and on, respectively, by applying a voltage V of (b) 38 V resulting in an electric field F of around 12 V/nm and (c) $V = 80$ V and $F \approx 25$ V/nm.

surface [cf. Figs. 1(b) and 1(c)]. In Fig. 1(b), at an applied voltage of 38 V, corresponding to an electric field of around 12 V/nm, the apex of the nanocone remained crystalline (see the fast Fourier transformation in Fig. S2(p) [27]). After increasing the electric-field strength to around 25 V/nm, the outmost atomic surface layers switched from a crystalline to a noncrystalline and disordered phase (see Fig. 1(c) and the discussion in Fig. S2 [27]).

There are several observations reported in the literature of a phase between solid and liquid, similarly to what we observe here. Additionally, there is a multitude of terms and expressions for what appears to be the corresponding phase. For example, a disordered surface layer has been referred to as surface melted layer [14], a quasiliquid [9,10], a coexisting solid-liquid phase [15,28], and surface roughening [11]. We are referring to the phase reported here as "surface roughening" or "disordered phase."

In order to rule out that the observed order-disorder transition occurred due to the high mobility of Au atoms at the tip or temperature effects, we compared the mobility of the atoms in the presence and absence of both the electron beam and electric field, and estimated the temperature increase induced by the beam. In particular, the high degree of dangling bonds at a step can increase the Au atom mobility and cause a sharp tip to become shorter and blunter even without exposure to the electron beam [29]. The energy transferred from the incident electron beam can then further increase the mobility. Similarly, the temperature increase from the beam-specimen interaction could possibly affect the crystallinity of the nanocones.

During a 4 min long electron-beam exposure without electrical bias, we observed that the tip radius r of the Au nanocone remained constant but that the nanocone was shortened by 5 atomic layers caused by a redistribution of Au atoms by surface diffusion ($t = 0$–4 min in Fig. 2(a), and corresponding

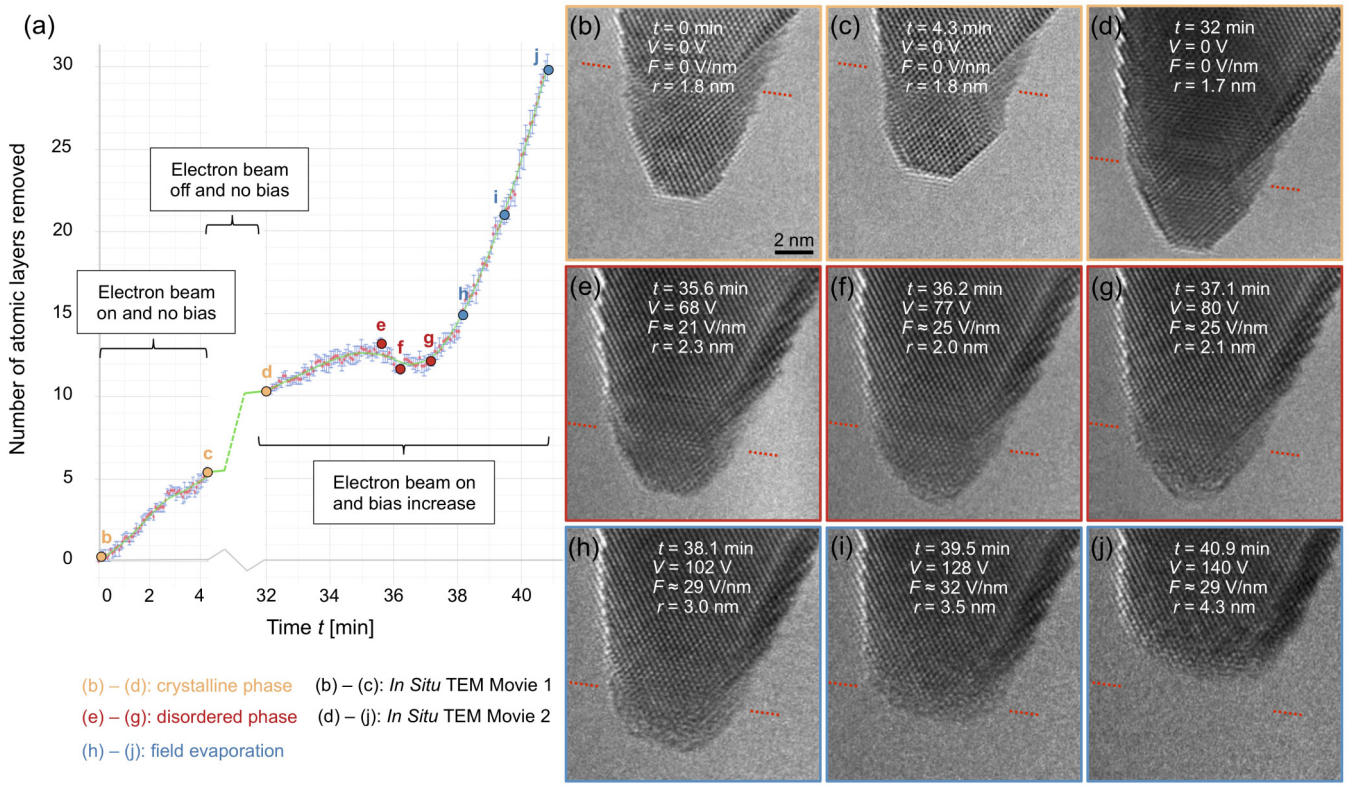

FIG. 2. Evolution of a Au nanocone apex under an electron beam and an intense electric field, from ordered to disordered to field-evaporated phase. (a) Number of atomic layers removed as a function of time t. (b)–(j) Extracted frames from *In Situ* TEM Movies 1 and 2 in Supplemental Material [27], corresponding to the points labeled b–j in (a). In the first and crystalline regime [orange, (b)–(d)], no electrical bias was applied and the electron beam was first turned on, then off, and then turned on again (note the truncated x axis); in the second and disordered regime [red, (e)–(g)], the electron beam was on and a bias from 68 to 80 V was applied; in the third regime [blue, (h)–(j)], the electron beam was on and the external bias was increased until field evaporation occurred (102–140 V). The error bars in (a), with an average height of 0.9 atomic layers, represent the uncertainty in measuring the number of atomic layers. V, F, and r denote the applied voltage, the corresponding electric field, and the tip radius, respectively. The red dotted lines in (b)–(j) mark points of reference. The scale bar in (b) also applies to (c)–(j).

Figs. 2(b) and 2(c) extracted from *In Situ* TEM Movie 1 in Supplemental Material [27]). After having the beam turned off for 28 min [$t = 4$–32 min in Fig. 2(a)], redistribution of atoms resulted in a shortening of the nanocone by another 5 atomic layers [Fig. 2(d)]. Hence, the electron beam was found to give rise to an increase of the atom diffusion rate by a factor of about 7, but it was not observed to affect the crystallinity of the nanocone [cf. Figs. 2(b) and 2(c)].

The temperature increase that was induced by the electron beam could be estimated through the increase of the atomic diffusion rate using the Arrhenius equation

$$k = A\mathrm{e}^{-(E_a/RT)}, \tag{1}$$

where k is the diffusion rate, A is the preexponential factor, E_a is the activation energy, R is the gas constant, and T is the temperature. Using Eq. (1), the sample temperature under the beam can be expressed as

$$T_{\mathrm{on}} = \frac{E_a}{R\left(\ln\frac{k_{\mathrm{off}}}{k_{\mathrm{on}}} + \frac{E_a}{RT_{\mathrm{off}}}\right)} = 317.5 \pm 3.5\ \mathrm{K},$$

with the subscripts "off" indicating the absence, and "on" the presence of the electron beam, and with the Au surface diffusion activation energy $E_a = 8.7864 \times 10^4\ \mathrm{J/mol}$ [30], $T_{\mathrm{off}} = 300\ \mathrm{K}$, and $R = 8.314\ \mathrm{J\,mol^{-1}\,K^{-1}}$. Thus, the 300 keV electron beam leads to an increase of the temperature of the nanocone by 17.5 ± 3.5 K, taking into account the same uncertainty as in the number of removed atomic layers [the same as the error bars in Fig. 2(a)]. Such a small temperature increase is expected to have a negligible effect on the emergence of a disordered phase and on the order-disorder switching, considering the significantly higher melting temperature (700–800 K) of Au nanoparticles [31].

Consequently, only upon application of an electrical bias to the nanocone, which was increased from 0 to 80 V ($t = 32$–37 min in Fig. 2(a), and corresponding Figs. 2(d) to 2(g) extracted from *In Situ* TEM Movie 2 in Supplemental Material [27]), the development of a disordered phase could be observed. The disordered phase started to appear at an electrical bias of 68 V [Fig. 2(e)], and at 77 and 80 V (Figs. 2(f) and 2(g), respectively), some of the outmost atomic layers were found to enter a disordered phase. Between 68 and 77 V, a slight decrease in the tip radius from 2.3 to 2.0 nm was observed [Figs. 2(e), 2(f), and the dip in the graph at $t = 36$ min in Fig. 2(a)], which is assumed to be owing to the increased mobility of the atoms in the electric field that momentarily sharpens the tip.

Notably, the order-disorder switching was found to be fully reversible using voltage control. The reversibility is seen as a

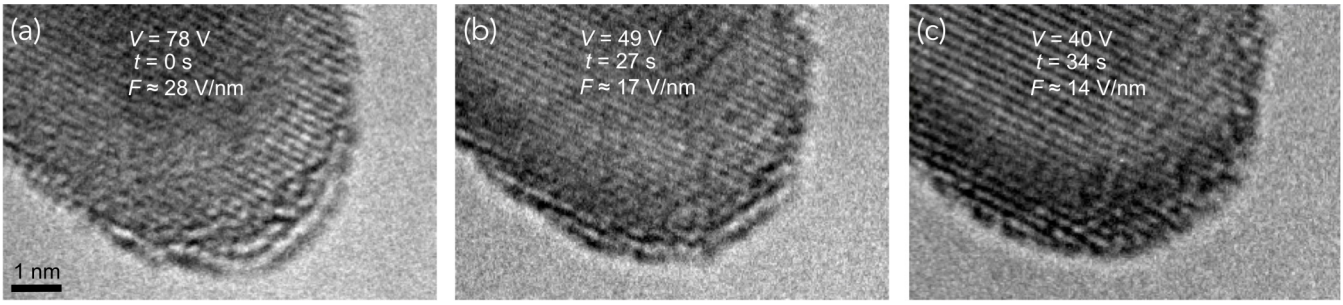

FIG. 3. Reversibility, from disordered to ordered during voltage decrease. The apex of a Au nanocone (different from the nanocone in Figs. 1 and 2) with tip radius of 2.5 nm and distance to cathode of 58 nm at different voltages. (a) The outmost layers are in a disordered phase, at an applied bias V of 78 V and an electric field F of around 28 V/nm. (b) 27 s after (a), with $V = 49$ V and $F \approx 17$ V/nm, some of the outmost layers remain in a disordered phase and in (c), 7 s later, the nanocone has reverted to a crystalline phase, at a bias of 40 V and an electric field of around 14 V/nm.

recrystallization of the disordered layers as the electric field is decreased (Fig. 3, extracted frames from *In Situ* TEM Movie 4 in Supplemental Material [27]). This was achieved on a different Au nanocone as the one shown in Figs. 1(b), 1(c), and 2 (thus also demonstrating the reproducibility of the electric-field-controlled order-disorder transition). In Fig. 3(a) a voltage $V = 78$ V and an electric field F of around 28 V/nm is applied to the nanocone and the outmost atomic layers are in a disordered phase. In Fig. 3(b) and 27 s later, $V = 49$ V and $F \approx 17$ V/nm with the disordered phase still being present. In Fig. 3(c) and 7 s later, at $V = 40$ V and $F \approx 14$ V/nm, the disordered layers have returned to their original state, from the decrease in the applied voltage. In the beginning of *In Situ* TEM Movie 4 the voltage is kept constant and above the disordering threshold, with the disordered layers remaining unchanged. That is, the disordered layers neither evaporate nor recrystallize at a constant voltage. Only in the second part of the movie, when the voltage is decreased, do the disordered layers recrystallize.

To distinguish the observed order-disorder switching from field evaporation of the surface layers, we investigated the structure and size of the first nanocone (i.e., not the nanocone in Fig. 3 that we demonstrated reversibility on) also at higher electrical biases of up to 140 V [$t = 38$–41 min in Fig. 2(a), and corresponding Figs. 2(h)–2(j)]. We found that the Au atoms of the disordered phase started to field-evaporate at an electrical bias of just below 102 V, corresponding to an electric field of around 29 V/nm [Fig. 2(h)]. Overall, the number of atomic layers removed increased sharply in the field-evaporation regime [$t = 38$–41 min in Fig. 2(a)] compared to at lower or no electrical biases. During this period, the nanocone experienced a shortening with around 18 atomic layers, and a broadening with an increase in the tip radius from 3.0 to 4.3 nm [Figs. 2(h)–2(j)]. Although the disordered layers evaporated, new disordered layers were immediately formed from the next atomic layer in the crystal. As a clarification, evaporation occurred when increasing the bias, whereas the recrystallization mentioned before occurred when the bias was decreased.

In order to obtain deeper understanding of the mechanism and temperature dependence of the observed electric-field-induced order-disorder transition, we conducted a series of atomic-scale simulations based on density functional theory (see Methods in Supplemental Material for details [27]). This approach accounts for charge redistribution and screening at the surface at a quantum-mechanical level. The objective is to be as predictive as possible and minimize ambiguities due to approximations intrinsic to resort to semiempirical models [32,33].

As a first step, we determined the field-evaporation threshold from *ab initio* molecular dynamics (AIMD) simulations. To this end, we followed the evolution of an atomistic tip model composed of 192 atoms at different constant external electric fields at 300 K. The AIMD simulations revealed an onset of evaporation at a field strength of around 25 V/nm, which is in good agreement with the experimental observations (see AIMD Movie 3 in Supplemental Material [27]). These initial simulations, however, failed to show disordering, which is not surprising given the constraint on the atomic geometry due to the fixed bottom layer in these simulations (Discussion 5 in Supplemental Material [27]).

Given the experimental observation of surface disorder at large fields, one might suspect that the electric field causes a softening of the bonds at the surface, leading to much larger thermal displacements. This would effectively suggest a form of surface melting in analogy to the Lindemann criterion, which formulates an empirical relation between the melting point and the mean square displacement of the atoms [13]. To test this hypothesis, we investigated the relaxation, charge distribution, and atomic thermal displacements at planar {111} Au surfaces under the influence of an external electric field (Fig. S4 [27]). The large density of states at the Fermi energy gives rise to a strong dielectric response, which very effectively screens the external electric field. Therefore, even for the largest field strengths of over 30 V/nm considered here, the external field barely penetrates more than one or two atomic layers [Fig. S4(d)]. While the top layer is strongly affected by the field, already the third—and for smaller field strengths even the second layer—exhibits bulk behavior. The localization of the excess charge at the topmost surface layer causes an outward relaxation of about 1% at a field strength of 30 V/nm [Fig. S4(a)]. The thermal displacements are indeed enhanced for the first layer and at a field of 26 V/nm, the thermal displacements at 300 K are 25% larger than in the field-free case. This is, however, only equivalent to a temperature increase of about 100 K under field-free conditions and thus insufficient to explain the experimental observation [Fig. S4(b)].

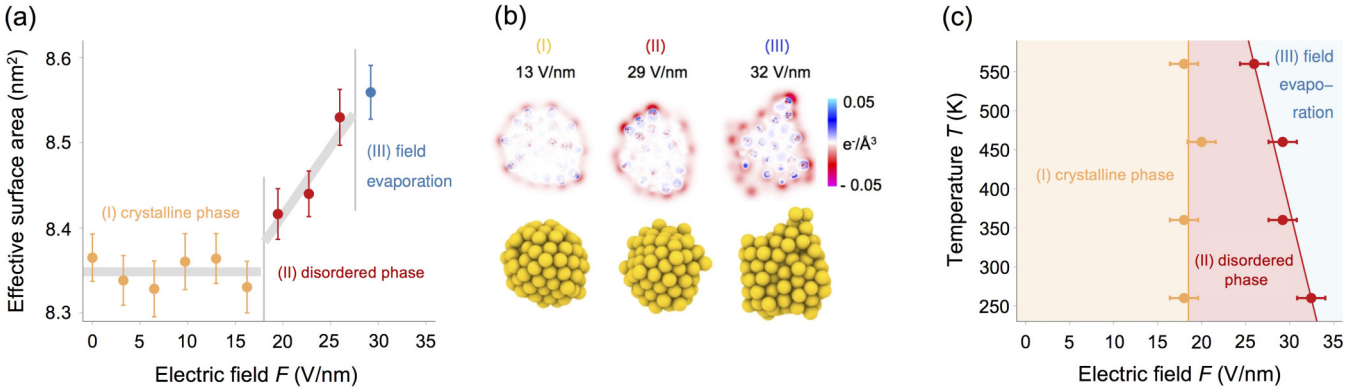

FIG. 4. *Ab initio* simulations of the crystalline phase, the disordered phase, and of field evaporation. (a) Effective surface area of a gold nanoparticle at 360 K as a function of the electric field. (b) Excess charge distribution (top) and shape (bottom) for three gold nanoparticles representative of the three stages indicated in (a). The color scale indicates the accumulation (light blue, maximum of 0.05 electrons/Å^3) and depletion (cerise, minimum of -0.05 electrons/Å^3) of electronic charge. (c) Approximate phase diagram showing the temperature dependence of the electric fields at which disordering (II) and field evaporation (III) occur.

To overcome the limitations imposed by the geometrical constraints intrinsic to tip model and extended surfaces (Discussion 5 in Supplemental Material [27]), we considered the behavior of small Au nanoparticles containing 135 atoms as a function of temperature and field strength. This allowed us to study the surface evolution not only without geometric constraints, but simultaneously to explore a reasonably wide range of temperatures and field strengths. The simulations showed that the electric field induced a very pronounced atomically localized charging of the surface [Fig. 4(b)]. At low to modest field strengths, the particles retained a spherical shape with an approximately constant surface area (stage I in Fig. 4 and AIMD Movie 1 in Supplemental Material [27]). If the field strength exceeded 18 V/nm, the particles elongated and displayed pronounced surface modes leading to a steady increase of the surface area with increasing field strength (stage II in Fig. 4). This change was accompanied by surface disordering and the localization of excess charge at individual surface atoms protruding from the surface [top row in Fig. 4(b)]. The shape elongation along with the occurrence of individual atoms at the surface support the hypothesis that the observed transition can be understood as a form of surface roughening, making it more energetically favorable to form surface defects. Ultimately, if the field strength was increased further, field evaporation took place (stage III in Fig. 4, AIMD Movie 2 [27]) as observed experimentally.

Although phase transitions in few-atom systems are often difficult to detect, here, the pronounced variation of the surface area with electric field provides a clear indication. Using the change in surface area [Fig. 4(a)], we can extract the surface roughening (the disordered phase) onset field and the field-evaporation threshold as a function of temperature [Fig. 4(c)]. While the roughening transition appears to be relatively insensitive to temperature at 18 V/nm, the field-evaporation threshold is found to decrease from 33 to 28 V/nm between 260 and 560 K, which is in semiquantitative agreement with previous experimental data [34]. Given the simplifications intrinsic to the simulations, in particular the use of nanoparticles, the agreement of the onset fields for disordering and evaporation with the experiments is remarkable. In all, these findings suggest a generality of electric-field-induced surface disorder also for other types of nanostructures and metals.

In summary, we have reported an electric-field-controlled and reversible order-disorder switching mechanism of the topmost atomic layers of Au nanocones, which was experimentally observed with atomic resolution using *in situ* TEM and confirmed by *ab initio* simulations. The switching is contactless, which has several advantages over switching by direct contact, e.g., avoiding mechanical wear and stress on a contact. The switching occurs at high electric fields that are difficult to reach using planar surfaces. Typically, nanometer-sized apices greatly enhance the electric fields [23], as for the Au nanocones. Therefore, to extend our results for larger regions, devices with varying length scales can be nanostructured using existing technologies for electronics and sensing. The findings suggest that the order-disorder transition can be seen as electric-field-induced surface roughening, providing fundamental understanding of atomic structural dynamics. Even though atom probe tomography operates at low temperatures [35], such knowledge is crucial for this and other nanomaterial characterization techniques dependent on intense electric fields (several large projects are aiming to combine atom probe tomography and TEM [36]). Of an immediate relevance is the external dynamic control of surface processes such as light-matter coupling via localized surfaces plasmons, which in noble metals typically are localized at a few atomic surface layers. With this work we uncover a technique for potentially steering the emergence, propagation, and routing of such surface-bound optical modes. This would have broad implications for nanophotonics, nanophotocatalysis, and other light-driven processes at the nanoscale. Moreover, the deterministic manipulation of the crystallinity of surface layers in nanostructures could be utilized in active nanodevices for various applications in field-effect transistor technology, catalysis, and sensor technology, as well as in studies addressing fundamental aspects in surface physics, material science, and low-dimensional phases of matter.

This work was supported by the European Network for Electron Microscopy (ESTEEM2, European Union Seventh Framework Program under Grant Agreement 312483-ESTEEM2

(Integrated Infrastructure Initiative–I3)), the Knut and Alice Wallenberg foundation, the Swedish Research Council and the Excellence Initiative Nano at Chalmers University of Technology.

L.d.K. and M.J.K. contributed equally to this work. L.d.K. and E.O. designed and conceived the experiment. L.d.K. carried out the experiment and the finite-element method simulations. M.J.K and J.L performed the molecular dynamics and density functional theory simulations. K.L fabricated the sample. L.d.K. prepared the manuscript. All authors discussed the results and contributed to writing the manuscript.

[1] M. Haruta, Catal. Today **36**, 153 (1997).

[2] M. Liu, Y. Pang, B. Zhang, P. De Luna, O. Voznyy, J. Xu, X. Zheng, C. T. Dinh, F. Fan, C. Cao, F. P. G. de Arquer, T. S. Safaei, A. Mepham, A. Klinkova, E. Kumacheva, T. Filleter, D. Sinton, S. O. Kelley, and E. H. Sargent, Nature (London) **537**, 382 (2016).

[3] *Nanoplasmonic Sensors*, edited by A. Dmitriev (Springer Science & Business Media, New York, 2012).

[4] L. Novotny and B. Hecht, *Principles of Nano-Optics* (Cambridge University Press, Cambridge, England, 2012).

[5] D. R. Hekstra, K. I. White, M. A. Socolich, and R. W. Henning, Nature (London) **540**, 400 (2016).

[6] B. Kasemo, Surf. Sci. **500**, 656 (2002).

[7] G. Xu, J. Abbott, L. Qin, K. Y. M. Yeung, Y. Song, H. Yoon, J. Kong, and D. Ham, Nat. Commun. **5**, 4866 (2014).

[8] A. H. Flood, J. F. Stoddart, D. W. Steuerman, and J. R. Heath, Science **306**, 2055 (2004).

[9] B. Pluis, A. W. Denier van derGon, J. W. M. Frenken, and J. F. van der Veen, Phys. Rev. Lett. **59**, 2678 (1987).

[10] A. Hoss, M. Nold, P. von Blanckenhagen, and O. Meyer, Phys. Rev. B **45**, 8714 (1992).

[11] A. S. Barnard, N. P. Young, A. I. Kirkland, M. A. van Huis, and H. Xu, ACS Nano **3**, 1431 (2009).

[12] M. Faraday, Proc. R. Soc. London **10**, 440 (1859).

[13] F. A. Lindemann, Phys. Z. **11**, 609 (1910).

[14] J. W. M. Frenken and J. F. van der Veen, Phys. Rev. Lett. **54**, 134 (1985).

[15] N. P. Young, M. A. van Huis, H. W. Zandbergen, H. Xu, and A. I. Kirkland, Ultramicroscopy **110**, 506 (2010).

[16] E. W. Müller, Z. Phys. **131**, 136 (1951).

[17] E. W. Müller, J. A. Panitz, and S. B. McLane, Rev. Sci. Instrum. **39**, 83 (1968).

[18] T. T. Tsong, Phys. Today **46**(5), 24 (1993).

[19] V. T. Binh and N. Garcia, J. Phys. I **1**, 605 (1991).

[20] K. J. Terhune, L. B. King, K. He, and J. Cumings, Nanotechnology **27**, 375701 (2016).

[21] K. A. Dean, T. P. Burgin, and B. R. Chalamala, Appl. Phys. Lett. **79**, 1873 (2001).

[22] M. S. Wang, L. M. Peng, J. Y. Wang, and Q. Chen, J. Phys. Chem. B **109**, 110 (2005).

[23] L. de Knoop, F. Houdellier, C. Gatel, A. Masseboeuf, M. Monthioux, and M. J. Hÿtch, Micron **63**, 2 (2014).

[24] A. V. Crewe, D. N. Eggenberger, J. Wall, and L. M. Welter, Rev. Sci. Instrum. **39**, 576 (1968).

[25] K. Svensson, Y. Jompol, H. Olin, and E. Olsson, Rev. Sci. Instrum. **74**, 4945 (2003).

[26] K. Lodewijks, V. Miljkovic, I. Massiot, A. Mekonnen, R. Verre, E. Olsson, and A. Dmitriev, Sci. Rep. **6**, 1 (2016).

[27] See Supplemental Material at http://link.aps.org/supplemental/10.1103/PhysRevMaterials.2.085006 that includes Methods (experimental and computational details), Supplemental Discussions 1–5, Supplemental Figures S1–S4, and 7 Movies with corresponding movie captions.

[28] D. Schebarchov and S. C. Hendy, J. Chem. Phys. **123**, 104701 (2005).

[29] G. Binnig and H. Rohrer, Rev. Mod. Phys. **59**, 615 (1987).

[30] T.-S. Lin and Y.-W. Chung, Surf. Sci. **207**, 539 (1989).

[31] P. Buffat and J.-P. Borel, Phys. Rev. A **13**, 2287 (1976).

[32] S. Parviainen, F. Djurabekova, S. P. Fitzgerald, A. Ruzibaev, and K. Nordlund, J. Phys. D: Appl. Phys. **49**, 045302 (2016).

[33] D. Beinke, C. Oberdorfer, and G. Schmitz, Ultramicroscopy **165**, 34 (2016).

[34] G. Schmitz, in *Nanotechnology* (Wiley-VCH Verlag, Weinheim, Germany, 2010), pp. 213–257.

[35] D. Blavette, A. Bostel, J. M. Sarrau, B. Deconihout, and A. Menand, Nature (London) **363**, 432 (1993).

[36] T. F. Kelly, Microsc. Microanal. **23**, 34 (2017).